Available online at www.sciencedirect.com
ScienceDirect
Journal of the European Ceramic Society 31 (2011) 1465–1471
www.elsevier.com/locate/jeurceramsoc

Phase, microstructure evolution and sintering of Sr-doped TiB_2 precursors

Ľuboš Bača [a,*], Zoltán Lenčéš [b], Nils Stelzer [a]

[a] *AIT Austrian Institute of Technology GmbH, Advanced Materials and Aerospace Technologies, A-2444 Seibersdorf, Austria*
[b] *Institute of Inorganic Chemistry, Slovak Academy of Sciences, Dúbravská cesta 9, SK-845 36 Bratislava, Slovakia*

Received 31 August 2010; received in revised form 10 January 2011; accepted 16 February 2011
Available online 15 March 2011

Abstract

Precursors for the preparation of bulk Sr-doped TiB_2 composites were synthesized by modified Pechini method. The high temperature behaviour of homogeneous Sr–Ti–B–C–O gels was investigated in the range 1200–1650 °C. DTA-TG analysis of the precursor powder shows two steps of the carbothermal reduction with endothermic peaks at temperatures of 1335 °C and 1500 °C. The influence of strontium content (2, 5, 10, 20 and 50 mol.%) on the phase composition and morphology of powders at 1650 °C was studied.

Due to the shift of TiB_2 diffractions and the detection of strontium in TiB_2 grains by EDX analysis the formation of $Ti_{1-x}Sr_xB_2$ solid solution is assumed in the Sr-doped powders. Finally, Sr-doped TiB_2 composites were inductive hot-pressed from the as prepared powders at 1900 °C for 7 min. The formation of $SrTiO_3$ phase in the powders is serving as a sintering aid during the preparation of bulk Sr–Ti–B composites. The exaggerated grain growth (grain size up to ~60 μm) occurs during the sintering with increasing content of strontium in the precursor.
© 2011 Elsevier Ltd. All rights reserved.

Keywords: Borides; Powders-chemical preparation; Sol–gel processes; TiB_2

1. Introduction

Generally, binary borides have been studied extensively since they exhibit excellent mechanical properties or various strongly correlated electron system features depending on the element bonded with the boron. The first category of borides represents metal diborides with excellent mechanical and good electrical and thermal properties e.g. TiB_2, ZrB_2 or HfB_2. The most popular and wide spread used metal diboride is TiB_2 with the Vickers hardness of 33 GPa, Young's modulus of 545 GPa, thermal conductivity of 64 W/mK and electrical resistivity 20.4 μΩ·cm at 25 °C.[1–3]

The second group of borides represented by alkaline earth borides of Ca, Sr or Ba crystallize in structures typical of *d* and *f* transition metal borides and have similar properties to rare-earth metal borides.[4–6] The divalent alkaline-earth hexaborides are investigated due to the properties such as high Curie temperature ferromagnetic semiconductors[7] and also for their thermoelectric properties with very favorable Seebeck coefficients and electrical conductivities, which make them potentially attractive for high-temperature thermoelectric (TE) applications.[8,9]

The structures of borides with lower boron content are determined by their metallic lattices, and the structures of higher borides by their boron atoms, which form strong sublattices with pronounced B–B bonds. The electrons in a boride of the first group are transferred to the metal, the main role in electronic structure being played by metallic states and in interatomic bonds by Me–Me bonds. In the case of higher borides the electrons are transferred to the boron sublattice, the main role in electronic structure and interatomic bonds of the compound are played by the *sp* states of boron and by B–B bonds, respectively. Based on the properties of single metal borides, it is with great interest to develop a synthesis route for new ternary boride composites and explore their properties and possibility of further applications. Some attempts to improve specific properties (mechanical, thermoelectric and tribological) of mixed borides were already described, [10–15] however there are immense potentials for boron based nanostructures that further exploration is required.

The excellent mechanical properties of TiB_2 combined with the thermoelectrical properties of SrB_6 could form a basis for the development of new ternary borides with enhanced mechanical

* Corresponding author. Tel.: +43 0 2622 90550 310; fax: +43 0 2622 90550 99.
E-mail address: lubos.baca@aac-research.at (Ľ. Bača).

0955-2219/$ – see front matter © 2011 Elsevier Ltd. All rights reserved.
doi:10.1016/j.jeurceramsoc.2011.02.028

Table 1
Strontium content in the Sr–Ti–B–C–O precursors.

Sample	STB-0	STB-2	STB-5	STB-10	STB-20	STB-50
Sr content (mol.%)	0	2	5	10	20	50

and physical properties e.g. thermoelectric energy conversion at high temperatures.

This work is focused on the sol–gel synthesis of boron based preceramic precursors in the Sr–Ti–B–C–O system suitable for the fabrication of ternary Sr–Ti–B composites. The influence of Sr concentration on the phase and microstructural evolution of TiB_2 powders during pyrolysis up to 1650 °C was studied. From such prepared powders a bulk Sr-doped TiB_2 composites were prepared by inductive hot-pressing at 1900 °C.

2. Experimental

Sol–gel derived strontium doped titanium diboride (Sr–TiB_2) powders were prepared by carbothermal reduction of the stoichiometric mixture of $TiCl_4$ (99.9%, Acros Organics, Belgium) and B_2O_3 (Rio Tinto Borax, USA) with various doping concentrations of $Sr(NO_3)_2$. Citric acid (CA) and ethylene glycol (EG) were used to chelate and polymerize the inorganic precursors. The detailed procedure of precursor preparation is described elsewhere.[16] Briefly, the starting boron oxide and strontium nitrate were dissolved in water, whereas titanium tetrachloride was slowly added to the calculated amount of ethylene glycol. Both solutions were mixed together and ethylene glycol was added in CA:EG ratio of 2:3, to promote the polymerization during the evaporation of water. Such prepared gel was dried in the furnace at 150 °C for 1 h and then crushed in agate mortar. The list of Sr–Ti–B–C–O precursors studied in this work is summarized in Table 1.

The high temperature synthesis of crystalline powders was carried out in alumina tube furnace at different temperatures in flowing argon atmosphere. The mass changes and thermal effects of the Sr–Ti–B–C–O precursors were performed and recorded through the QMS 403 Aëolos® quadrupole mass spectrometer and NETZSCH STA 449 F1 Jupiter® thermal analyzer coupled with FTIR Tensor 27 (Bruker) spectrometer. Phase composition was identified by powder X-ray diffraction analysis (X-pert, Philips). Field emission scanning electron microscopy (FESEM, Carl Zeiss SUPRA^{TM} 40VP) was used to study the crystal size and morphology of Sr–Ti–B powders. EDX spectra were recorded to identify the chemistry of different morphologies obtained in the samples.

3. Results and discussion

3.1. DTA-TG and XRD analysis

Differential thermal analysis coupled with thermal gravimetry and mass spectroscopy (DTA-TG-MS) were used to identify the high temperature changes during the carbothermal reduction of Sr–Ti–B–C–O precursors. Based on the previous XRD and Raman results in Ti–B–C–O system,[16] where the annealing of precursors at 1100 °C shows only the formation of $TiBO_3$, rutile and graphite, thus the starting temperature of 1200 °C was selected for the first calcination of Sr-doped precursor. DTA-TG spectra of 1200 °C treated sample (STB-10, Table 1) were recorded up to 1600 °C in order to study the processes at higher temperatures. The gaseous by-products were identified with the help of MS-FTIR spectroscopy. The DTA-TG results presented in Fig. 1 shows three endothermic peaks during the heat treatment up to 1600 °C.

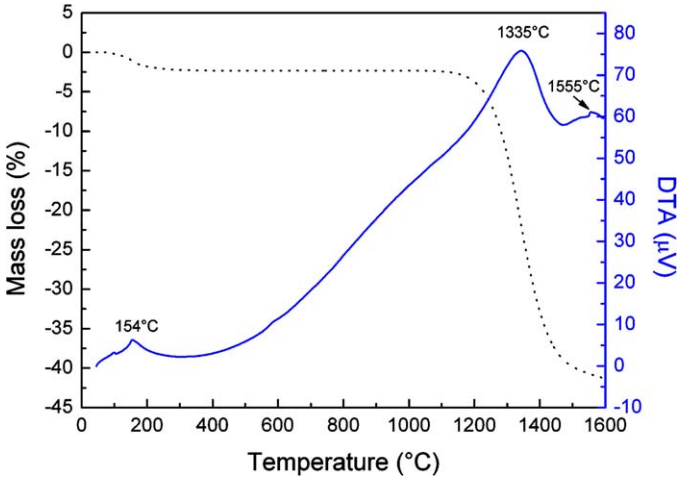

Fig. 1. DTA-TG analysis of sample STB-10, previously annealed at 1200 °C.

The first small peak at 154 °C is associated with the evaporation of adsorbed water. The second endothermic peak between 1200 °C and 1470 °C is associated with a high mass loss as it is shown in the TG curve. This mass loss is mainly caused by the evolution of CO during the carbothermal reduction of Sr–Ti–B–C–O precursor as it was also confirmed by the mass and FTIR spectroscopy (data not shown). The maximum of the carbon monoxide evolution was observed at 1335 °C. Finally, the weak endothermic peak observed at 1555 °C indicates the second stage of CO formation during the carbothermal reduction of Ti_2O_3 and SrB_2O_4 phases as it was confirmed by XRD analysis (Fig. 2).

The XRD analysis of the annealed product at 1200 °C showed the presence of TiC, TiB_2 and traces of TiO_2 crystalline phases. The phase analysis further showed that during the first stage of weight loss in the temperature range 1200–1300 °C the content of crystalline TiC phase decreased and finally disappeared at 1400 °C. At the same time the intensity of TiB_2 peaks increased and also Ti_2O_3 phase crystallized from the precursor at 1300 °C. It indicates that at lower temperatures TiC reacts with the amorphous boron to form TiB_2 according to reaction:

$$TiC(s) + 2B(s) = TiB_2(s) + C(s) \quad (1)$$

Free carbon formed *in situ* is then responsible for the first stage of precursor reduction. The phase analysis proposes the following reaction:

$$2TiO_2(s) + 2B(s) + C(s) = TiB_2(s) + Ti_2O_3(s) + CO(g) \quad (2)$$

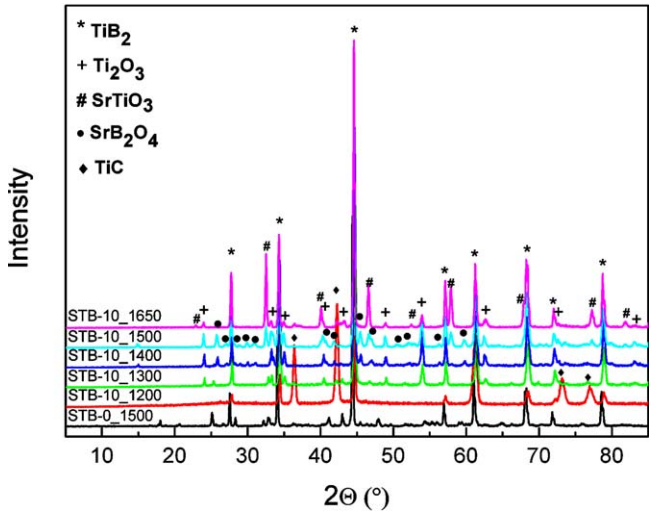

Fig. 2. XRD analysis of Sr–Ti–B–C–O precursors with 10 mol% Sr content after high temperature annealing. Sample STB-0-1500 is without strontium, annealed at 1500 °C.

The XRD analysis shows only the formation of SrB_2O_4 from the amorphous phase by crystallisation above 1300 °C except Ti-containing compounds (Fig. 3). According to the observed diffractogram SrB_2O_4 is present up to 1500 °C. The chemical reaction continues based on the phase analysis at higher temperatures ($T > 1500$ °C) as follows:

$$SrB_2O_4(s) + Ti_2O_3(s) + 4C(s) = TiB_2(s) + SrTiO_3(s) + 4CO(g) \quad (3)$$

The thermodynamic calculations (Malt-2 for Windows program and JANAF Thermodynamic database[17]) gave a Gibbs free energy of reaction (3) $\Delta G_r = -89.4\ kJ\ mol^{-1}$ at 1500 °C. This result also indicates that reaction (3) can proceed to the right at this temperature. The XRD analysis confirmed (Fig. 3) that the formed ferroelectric $SrTiO_3$ phase is stable up to the maximum annealing temperature 1650 °C that was applied in this work. This phase can serve as a sintering aid during the preparation of bulk Sr–Ti–B-based composites, and/or as a precursor for ternary boride formation, when sufficient carbon and boron is present.

Despite the lack of the thermodynamic data for SrB_6 it is assumed that at higher sintering temperatures in the excess of B and C, $SrTiO_3$ is reduced:

$$SrTiO_3(s) + 8B(s) + 3C(s) = SrB_6(s) + TiB_2(s) + 3CO(g) \quad (4)$$

In order to obtain more precise information about the behaviour of strontium in Sr–Ti–B–C–O system, new samples with various strontium contents were prepared (Table 1). Samples were annealed at 1650 °C for 3 h in argon atmosphere and analyzed by XRD analysis (Fig. 3).

The XRD patterns of samples doped with 5 and 10 mol.% Sr shows that the major phase is TiB_2 and the minor phases are Ti_2O_3 and $SrTiO_3$, respectively. In the samples with 10 mol.% Sr the intensity of the $SrTiO_3$ phase increases, whereas the intensity of Ti_2O_3 phase decreases compared to the sample with lower amount of strontium. Surprisingly, in the sample with the highest amount of strontium (50 mol.%), $SrTiO_3$ phase was not detected by XRD analysis and except TiB_2 and Ti_2O_3 only $Sr_2B_2O_5$ phase is present. The more detailed analysis of the XRD pattern showed the presence of some unidentified peaks associated with the positions of SrB_6 phase (JCPDS 28-1210), however the positions of these diffractions are shifted to higher angles by $\Delta(2\Theta) \approx 0.15°$.

The presence of other Sr-based oxide phases in the annealed precursors indicates the lack of carbon (formed by reaction (1)) in the system for the progress of reaction (3). In order to prove this assumption another sample STB-50-15C was prepared, i.e. the STB-50 sample was mixed with 15 wt.% excess of carbon black (Cabot Corp.) and heat treated at 1650 °C for 3 h in argon. The XRD pattern of this sample shows the main diffractions of TiB_2, SrB_6 and also a small amount of TiO (Fig. 4). When

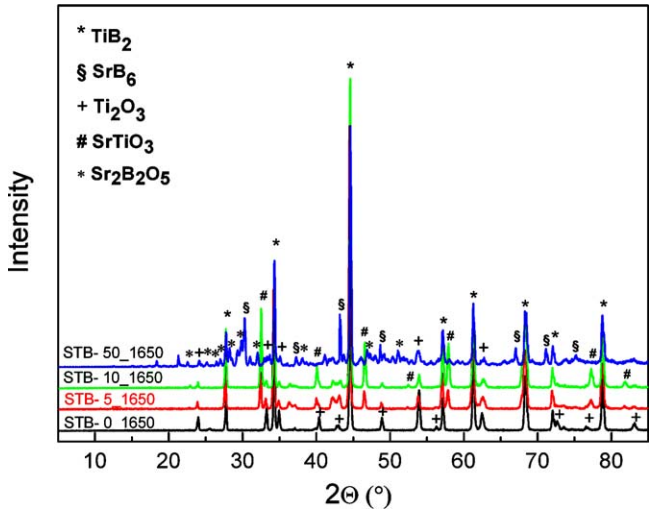

Fig. 3. Effect of strontium addition on the phase composition of Sr–Ti–B–C–O precursors annealed at 1650 °C for 3 h in argon.

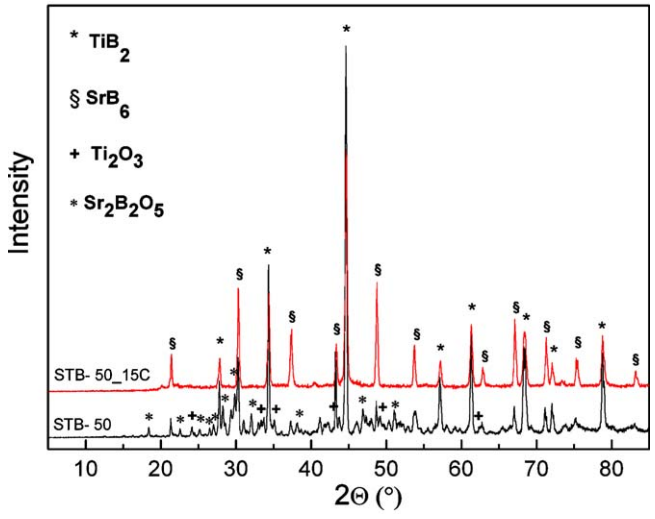

Fig. 4. Comparison of XRD patterns of stoichiometric Sr–Ti–B–C–O sample (STB-50-1650) and precursor with 15 wt.% excess carbon addition (STB-50-15C-1650) after annealing at 1650 °C for 3 h under argon atmosphere.

sufficient amount of carbon is present in the reaction system, the content of crystalline strontium and titanium oxide phases decreases to the negligible level and major phases TiB_2 and SrB_6 are formed.

Similar occurrence as for the SrB_6 peaks detected in STB-50 and STB-50-15C samples was also observed in the XRD patterns of STB-10 samples with stoichiometric amount of carbon but for TiB_2 diffractions which are shifted to higher 2Θ angles. These precise XRD measurements were conducted in Debye–Scherrer transmission geometry (STOE Stadi-P, Germany) with a step of 0.025°/min. The data were collected on a position-sensitive detector. The observed shift of TiB_2 diffractions suggests the formation of either nonstoichiometric $Ti_{1-x}B_2$, or most probably the formation of $Ti_{1-x}Sr_xB_2$ solid solution, because the EDX analysis showed the presence of strontium in the TiB_2 particles. Although the formation of mixed hexaborides[11,12] and diborides[18–20] is well studied, to our knowledge there is no report about the formation of Ti–Sr–B-based solid solution.

The deconvolution analysis of the (1 0 1) plane diffraction of Sr-doped TiB_2 (STB-10 sample annealed at 130 °C) shows that the diffraction maximum consists of at least two peaks (Fig. 5). The first major peak belongs to TiB_2, while the second one is unknown. Owing to the similar behaviour of Sr to Ca and Ba in a group of alkaline earth elements and the fact that calcium forms both the hexagonal CaB_2 and cubic CaB_6, and similarly BaB_2 transforms to more stable BaB_6,[21,22] the existence of metastable SrB_2 phase, or the formation of $Ti_{1-x}Sr_xB_2$ solid solution might be considered. Although only the SrB_6 is in the XRD database, Zajchowski et al.[23] mentioned the existence SrB_2 phase, but without any details regarding the structure and properties.

The formation of $Ti_{1-x}Sr_xB_2$ solid solution can proceed according to the following general reaction:

$$Me_nO_m + nB_2O_3 + (m+3n)C \rightarrow MeB_2 + (m+3n)CO \quad (5)$$

where $n=2$ and $m=3$ would be for Me = Ti, and $n=m=1$ would be for Me = Sr in the present studied system. The formation of thermodynamically stable SrB_6 phase at higher temperatures follows the reaction:[22]

$$Me_nO_m + 3nB_2O_3 + (m+9n)C \rightarrow MeB_6 + (m+9n)CO \quad (6)$$

with the same values of variables as in reaction (5). It is obvious that the formation of diborides requires lower amount of carbon, although except of this reducing agent the other controlling parameters like temperature, gas pressure and time play an important role.[24] In sample STB-50-15C with an excess of carbon reaction (6) can proceed and except of TiB_2 also SrB_6 is formed.

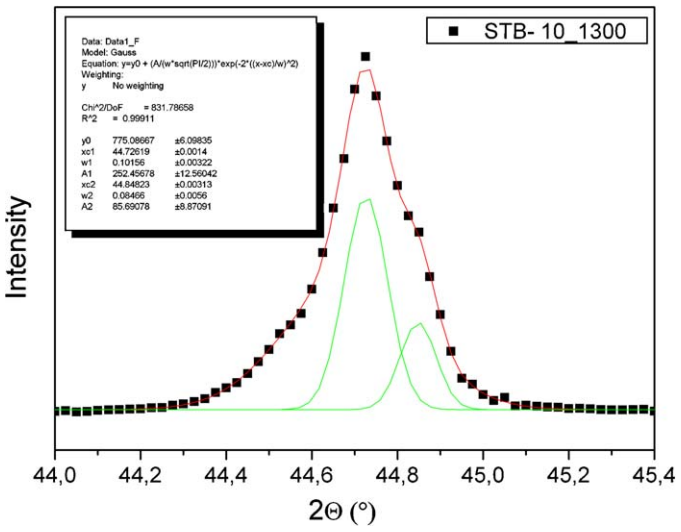

Fig. 5. Deconvolution of (1 0 1) plane diffraction of STB-10 sample.

3.2. SEM and EDX analysis

The microstructure evolution of heat treated sol–gel derived Sr–Ti–B–C–O precursors was investigated from 1200 °C up to 1650 °C for 3 h.

Three different morphologies were observed in the precursor after annealing at 1200 °C in flowing argon (Fig. 6a). The relatively large platelet-like grains TiB_2 particles with the size of 7–10 μm and thickness about 100 nm were observed. The smaller round-shaped grains with a diameter up to 3 μm were identified as TiC. The large amorphous areas (Fig. 6b) contain the remains of unreacted precursor, because no other crystalline phases were detected at this temperature by XRD analysis.

When the temperature reached 1300 °C in the previously amorphous areas small clusters of plate-like TiB_2 grains grew to the size of ~10 μm from the centre of area to all directions (Fig. 6c). At this temperature, the carbothermal reduction of precursor rises and new titanium oxide phase appears. However, XRD analysis shows no evidence of crystalline Sr-containing phases at 1300 °C.

With further temperature increase the amount of amorphous phase remarkably decreased what corresponds with the results of XRD and DTA-TG analysis (Fig. 6d). Based on the XRD, SEM and EDX analysis of all samples, it is assumed that during the calcinations a part of strontium ions are incorporated in the unreacted amorphous phase and part as the $Ti_{1-x}Sr_xB_2$ solid solution. We suppose that during the crystallization process the strontium content in the $Ti_{1-x}Sr_xB_2$ solid solution is modifying in the temperature dependent manner. The quantification of EDX spectra at different temperatures proves that the strontium content in the crystals varies (Fig. 7). However, this hypothesis will require a more detailed study of the Sr–Ti–B–C system.

Finally, the synthesised precursors were sintered at 1900 °C and the preliminary results showed that the preparation of dense Sr-doped TiB_2 composite can be done by inductive hot-pressing from the annealed powders (Table 2).

The density measurement revealed the highest bulk density for the sample doped with 2 mol.% of Sr (STB-2) followed by sample STB-0 and samples STB-5 and STB-10, respectively. As can be seen, the bulk density varies with the phase composition. XRD analysis of sintered STB-0 sample revealed the presence of TiB_2, TiC and a very low amount of Ti_2O_3 phase. Similar results were observed in the STB-5 sample (Fig. 8). Neither crystalline SrB_6, nor other Sr-based phases were identified. On the other

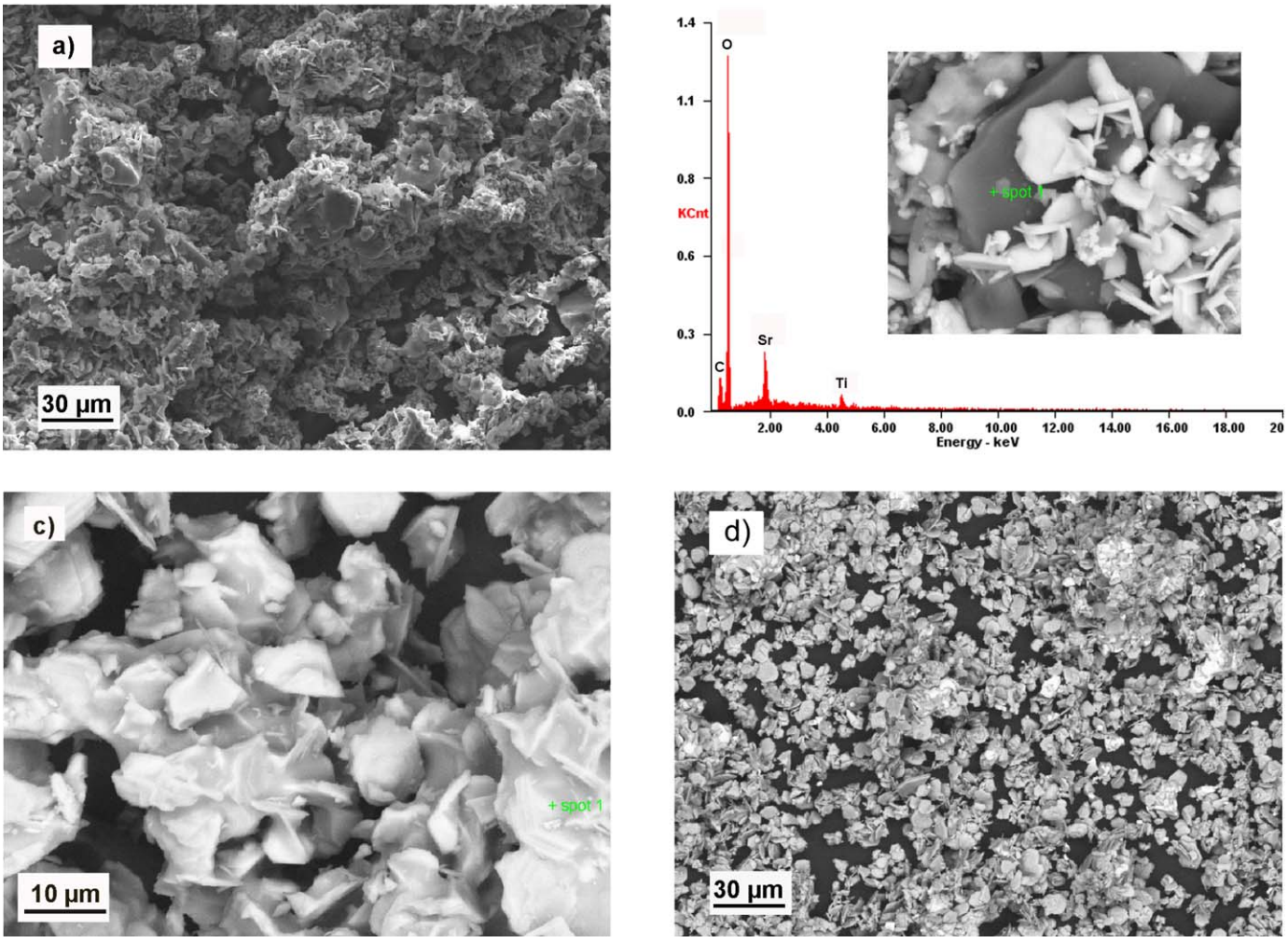

Fig. 6. Scanning electron micrographs of 10 mol.% Sr-doped TiB_2 powders calcined in flowing Ar atmosphere (a) at 1200 °C/3 h; (b) EDX analysis of this sample; and back scattered micrographs of samples annealed at (c) 1300 °C/3 h; (d) 1650 °C/3 h.

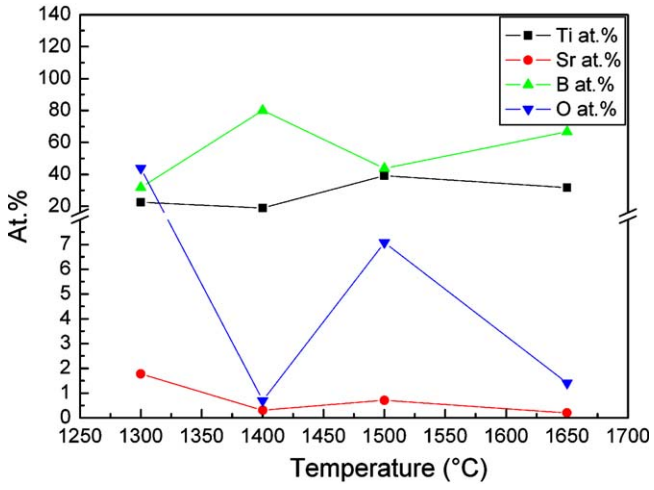

Fig. 7. The effect of temperature on the content of selected elements in STB-10 powder during the carbothermal reduction obtained from EDX analysis.

hand, XRD pattern of the bulk ceramic composite prepared from the STB-10 powder showed beside TiB_2 and TiC phases, also the presence of $SrTiO_3$ phase. The lack of carbon necessary for the reduction of $SrTiO_3$ (see reaction (4)) prevents the formation of SrB_6.

Table 2
Densities of hot pressed Sr-Ti-B-C-O samples with different Sr content.

Sample	STB-0	STB-2	STB-5	STB-10
Sr content (mol.%)	0	2	5	10
Bulk Density (g cm^{-3})	4.39	4.49	4.33	4.36

The morphology of samples was studied by employing of SEM on the fracture surfaces of the sintered samples (Fig. 9a–d). The micrographs show that the finest microstructure with the smallest particle size was obtained for the STB-2 sample. With addition of strontium in the precursor, the exaggerated grain growth occurs as it was seen in sample STB-10 with grain size up to ~60 µm. This grain size increase is explained by the higher amount of liquid phase during sintering. $SrTiO_3$ and other oxide impurities can form liquid phase during sintering at 1900 °C and thus enhance the sintering and also the grain growth process. During the rapid cooling crystalline $SrTiO_3$ or Ti_2O_3 phases re-precipitate from the liquid, supported by XRD patterns.

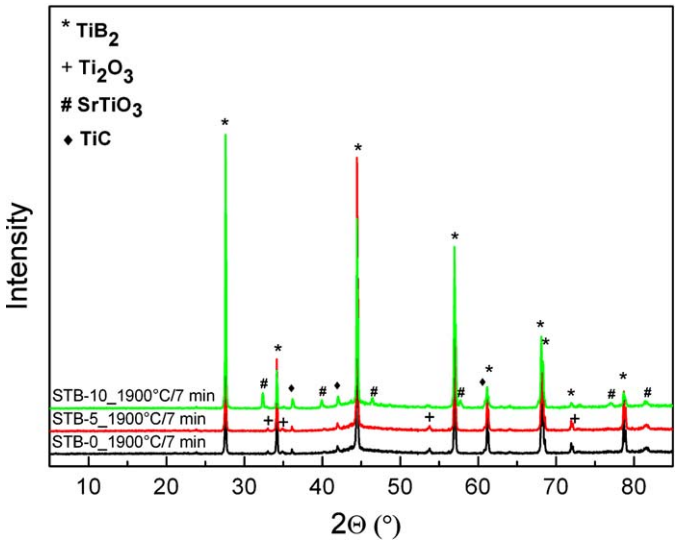

Fig. 8. XRD analysis of bulk Sr doped TiB2 ceramics prepared from precursors with 0, 5 and 10 mol.% Sr content (STB-0, STB-5, STB-10) after sintering at 1900 °C for 7 min by inductive hot pressing.

4. Conclusions

Sr-Ti-B precursor was successfully prepared from $TiCl_4$, B_2O_3 and $Sr(NO_3)_2$ mixture by modified Pechini process followed by subsequent annealing in the temperature range 1200–1650 °C. DTA-TG analysis coupled with mass spectroscopy showed two endothermic peaks at 1335 °C and 1555 °C associated with the carbothermal reduction of Sr–Ti–B–C–O precursor. XRD analysis revealed that during the first stage of reduction SrB_2O_4 and Ti_2O_3 phase is reduced according to reaction:

$$SrB_2O_4(s) + Ti_2O_3(s) + 4C(s) = TiB_2(s) + SrTiO_3(s) + 4CO(g)$$

The *in situ* formed $SrTiO_3$ phase can serve as a sintering aid during the preparation of bulk Sr–Ti–B-based composites, and/or as a precursor for ternary boride formation. When sufficient carbon and boron is present in the reaction system, the second stage of reduction proceeds above 1500 °C via reaction:

$$SrTiO_3(s) + 8B(s) + 3C(s) = SrB_6(s) + TiB_2(s) + 3CO(g)$$

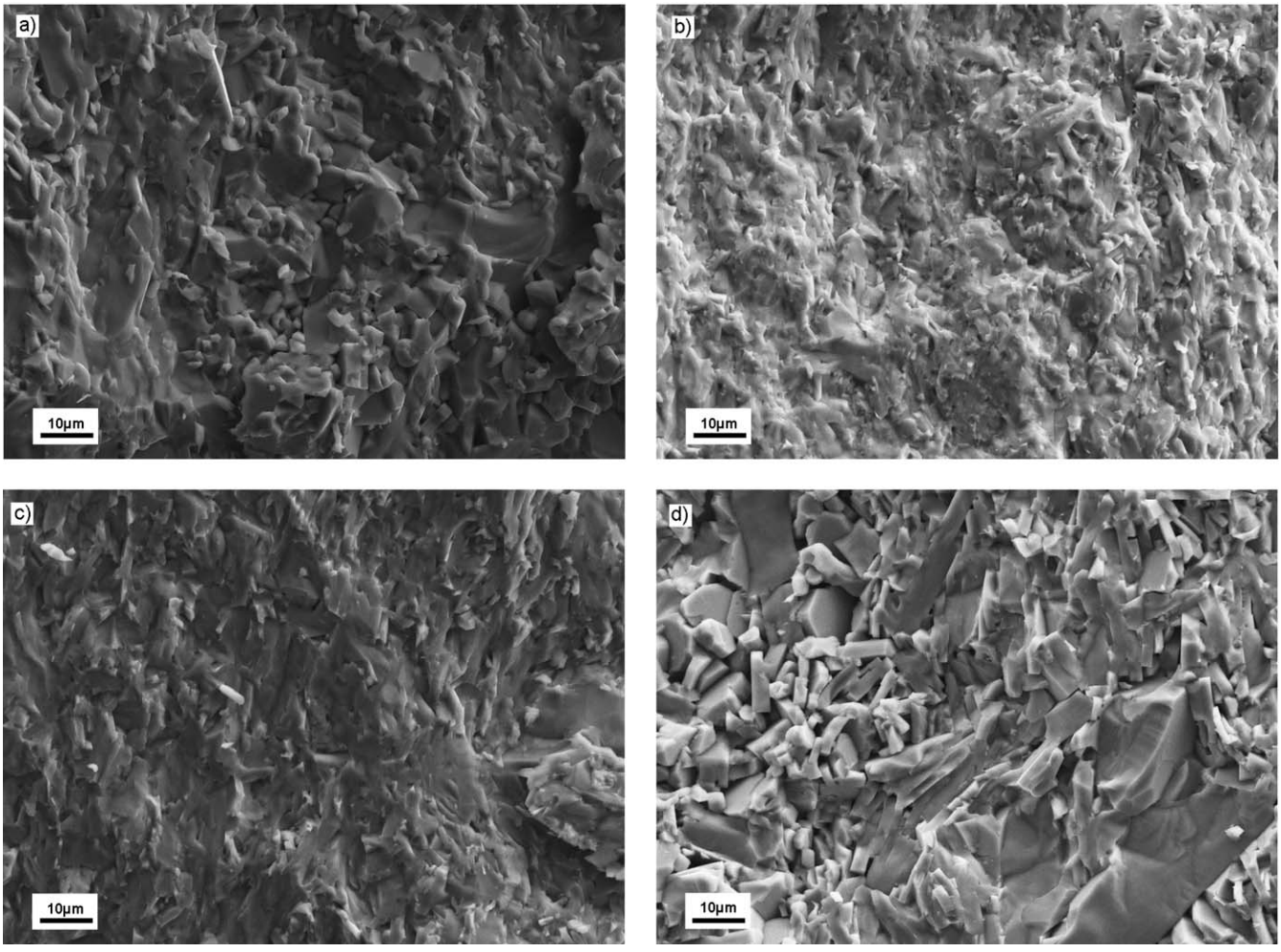

Fig. 9. Scanning electron micrographs of Sr-doped TiB2 bulk ceramics prepared from as synthesized Ti–Sr–B–O precursors by inductive hot-pressing at 1900 °C for 7 min in vacuum (a) STB-0; (b) STB-2 (c) STB-5; (d) STB-10.

The XRD analysis of products annealed at 1650 °C showed that the excess of carbon is necessary for the complete reduction of oxide phases and allows the formation of almost pure TiB_2–SrB_6 powder.

Relatively large platelet-like TiB_2 grains were growing to the size of ∼10 μm above 1300 °C from the remaining amorphous parts of the precursors to all directions.

Finally, the precursors were densified by inductive hot-pressing at 1900 °C for 7 min in argon atmosphere. During the sintering an exaggerated grain growth (grain size up to ∼60 μm) was observed, more pronounced with increasing content of strontium in the precursor. Samples with 2 mol.% of Sr achieved the highest density among the tested compositions.

Acknowledgement

The work was supported by the Slovak Grant Agency VEGA 2/0178/10.

References

1. Shackelford JF, Alexander W. *CRC materials science and engineering handbook*. 3rd ed. Boca Raton: CRC Press; 2001.
2. Baumgartner HR, Steiger RA. Sintering and properties of titanium diboride made from powder synthesized in a plasma-arc heater. *J Am Ceram Soc* 1984;**67**:207–12.
3. Rahman M, Wang CC, Chen W, Akbar SA. Electrical resistivity of titanium diboride and zirconium diboride. *J Am Ceram Soc* 1995;**78**:1380–2.
4. Samsonov GV, Serebryakova TI. Classification of borides. *Poroshkovaya Metatlurgiya* 1978;**2**(182):38–44.
5. Ott HR, Chernikov M, Felder E, Degiorgi L, Moshopoulou EG, Sarrao JL, et al. Structure and low temperature properties of SrB_6. *Z Phys B* 1997;**102**:337–45.
6. Jash P, Nicholls AW, Ruoff RS, Trenary M. Synthesis and characterization of single-crystal strontium hexaboride nanowires. *Nano Lett* 2008;**8**:3794–8.
7. Young DP, Hall D, Torelli ME, Fisk Z, Sarrao JL, Thompson JD, et al. High-temperature weak ferromagnetism in a low-density free-electron gas. *Nature* 1999;**397**:412–4.
8. Takeda M, Terui M, Takahashi N, Ueda N. Improvement of thermoelectric properties of alkaline-earth hexaborides. *J Solid State Chem* 2006;**179**:2823–6.
9. Dresselhaus MS, Chen G, Tang MY, Yang RG, Lee H, Wang DZ, et al. New directions for low-dimensional thermoelectric materials. *Adv Mater* 2007;**19**:1043.
10. Blitznakov G, Isolovski I, Pescher P. Investigation on cathode materials prepared from mixed metal hexaborides. *Rev Int Hautes Temp Refract* 1969;**6**:159–64.
11. Futamoto M, Nakazawa M, Kawabe U. High temperature surface composition of hexaboride thermionic electron emitters. *Vacuum* 1983;**33**:727–32.
12. Futamoto M, Nakazawa M, Kawabe U. Thermionic emission properties of hexaborides. *Surface Science* 1980;**100**:470–80.
13. Cook BA, Harringa JL, Lewis TL, Russell AM. A new class of ultra-hard materials based on $AlMgB_{14}$. *Scripta Mater* 2000;**42**:597–602.
14. Imai Y, Mukaida M, Ueda M, Watanabe A. Screening of the possible boron-based n-type thermoelectric conversion materials on the basis of the calculated densities of states of metal borides and doped β-boron. *Intermetallics* 2001;**9**(8):721–34.
15. Takeda M, Fukuda T, Domingo F, Miura T. Thermoelectric properties of some metal borides. *J Solid State Chem* 2004;**177**:471–5.
16. Bača L', Stelzer N. Adapting of sol–gel process for preparation of TiB_2 powder from low-cost precursors. *J Eur Ceram Soc* 2008;**28**:907–11.
17. Chase MW Jr. NIST-JANAF thermochemical tables. 4th ed. (Part I and Part II). *J Phys Chem Ref*, Monograph 9; 1998.
18. Zdaniewski WA. Solid solubility effect on properties of titanium diboride. *J Am Ceram Soc* 1987;**70**:793–7.
19. Shibuya M, Kawata M, Ohyanagi M. Titanium diboride-tungsten diboride solid solutions formed by induction-field-activated combustion synthesis. *J Am Ceram Soc* 2003;**85**:706–10.
20. Avilés MA, Córdoba JM, Sayagués MJ, Alcalá MD, Gotor FJ. Mechanosynthesis of $Hf_{1-x}Zr_xB_2$ solid solution and $Hf_{1-x}Zr_xB_2$/SiC composite powders. *J Am Ceram Soc* 2010;**93**:696–702.
21. Torkar K, Krischner H, Hitsch E. Preparation and identification of barium diboride. *Monatschefte für Chemie* 1972;**103**:744–50.
22. Markovskii LYa, Vekshina NV, Bezruk ET, Sukhareva GE, Voevodskaya TK. A magnesium-thermic method for the preparation of metal borides. *Poroshkovaya Metallurgia* 1969;**5**(77):13–8.
23. Zajchowski PH, Schlichting KW. Dispersion strengthened ceramic thermal barrier coating. *US Patent Application* No. 20090291323, class 428698; 2008.
24. Zheng S-Q, Zou Z-D, Min G-H, Yu H-S, Han J-D, Wang W-T. Synthesis of strontium hexaboride powder by the reaction of strontium carbonate with boron carbide and carbon. *J Mater Sci Lett* 2002;**21**:313–5.